Improving the Mg Sacrificial Anode in Tetrahydrofuran for Synthetic Electrochemistry by Tailoring Electrolyte Composition

Wendy Zhang,[†] Chaoxuan Gu,[‡] Yi Wang,[¶] Skyler D. Ware,[†]

Lingxiang Lu,[¶] Song Lin,[¶] Yue Qi,[‡] and Kimberly A. See[*,†]

†*Division of Chemistry and Chemical Engineering, California Institute of Technology, Pasadena, California 91125, United States*

‡*School of Engineering, Brown University, Providence, Rhode Island 02912, United States*

¶*Department of Chemistry and Chemical Biology, Cornell University, Ithaca, New York 14853, United States*

E-mail: ksee@caltech.edu

Supporting Information
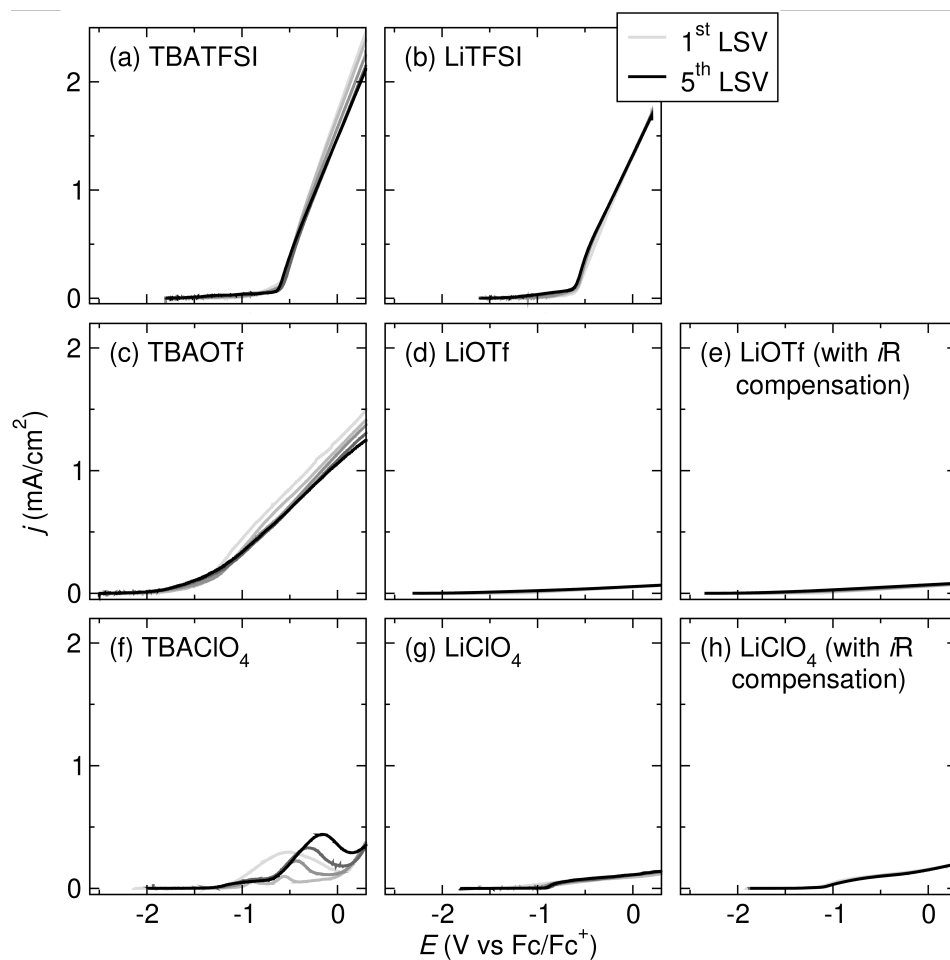
Linear sweep voltammograms of Mg stripping

Figure S1: Linear sweep voltammograms of Mg stripping in THF with TBA$^+$ and Li$^+$ supporting electrolytes. All voltammograms were collected at a scan rate of 5 mV s^{-1}. For each electrolyte, five LSVs were collected with a 10 min OCV between scans. For (e) and (h), the LSVs were collected with 85% iR compensation
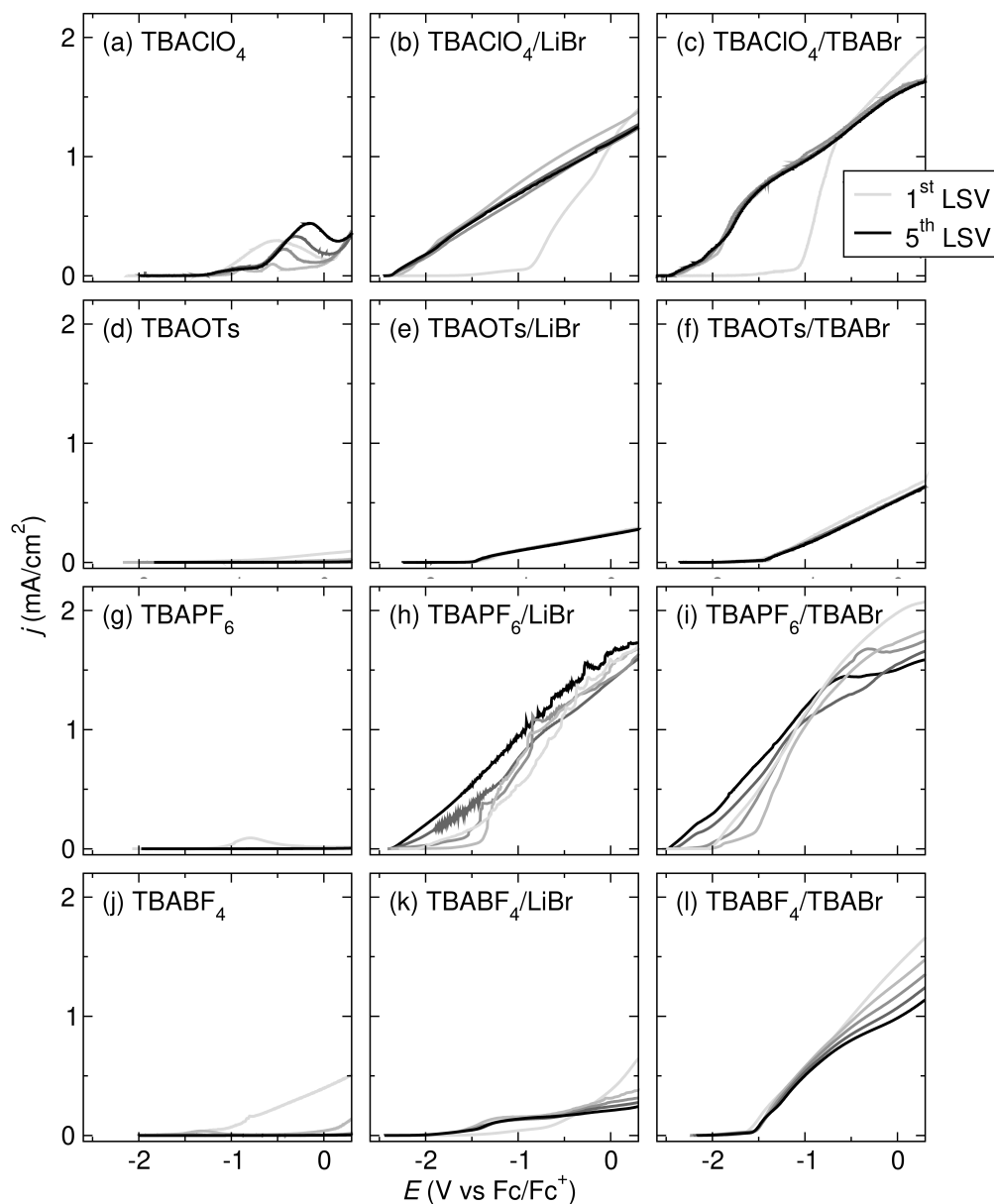
Figure S2: Linear sweep voltammograms of Mg stripping in THF with and without Br^- co-supporting electrolyte. All voltammograms were collected at a scan rate of 5 mV s^{-1}. For each electrolyte, five LSVs were collected with a 10 min OCV between scans.

Figure S3: Linear sweep voltammograms of Mg stripping in THF with TBAPF$_6$/LiX supporting electrolyte. All voltammograms were collected at a scan rate of 5 mV s^{-1}. For each electrolyte, five LSVs were collected with a 10 min OCV between scans.
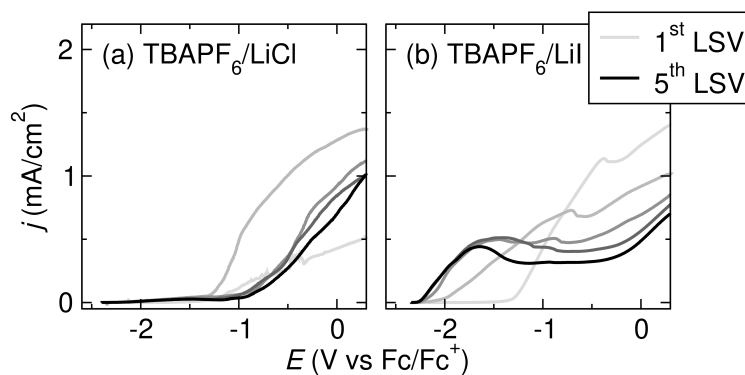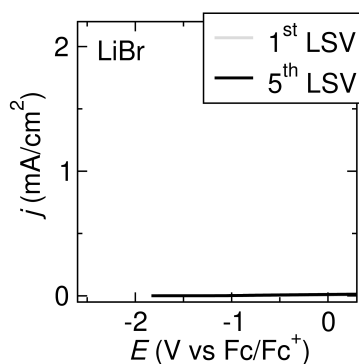

Figure S4: Linear sweep voltammograms of Mg stripping in THF with LiBr supporting electrolyte. All voltammograms were collected at a scan rate of 5 mV s^{-1}. For each electrolyte, five LSVs were collected with a 10 min OCV between scans. LSV in TBABr/THF was not collected due to the low solubility of TBABr in THF.
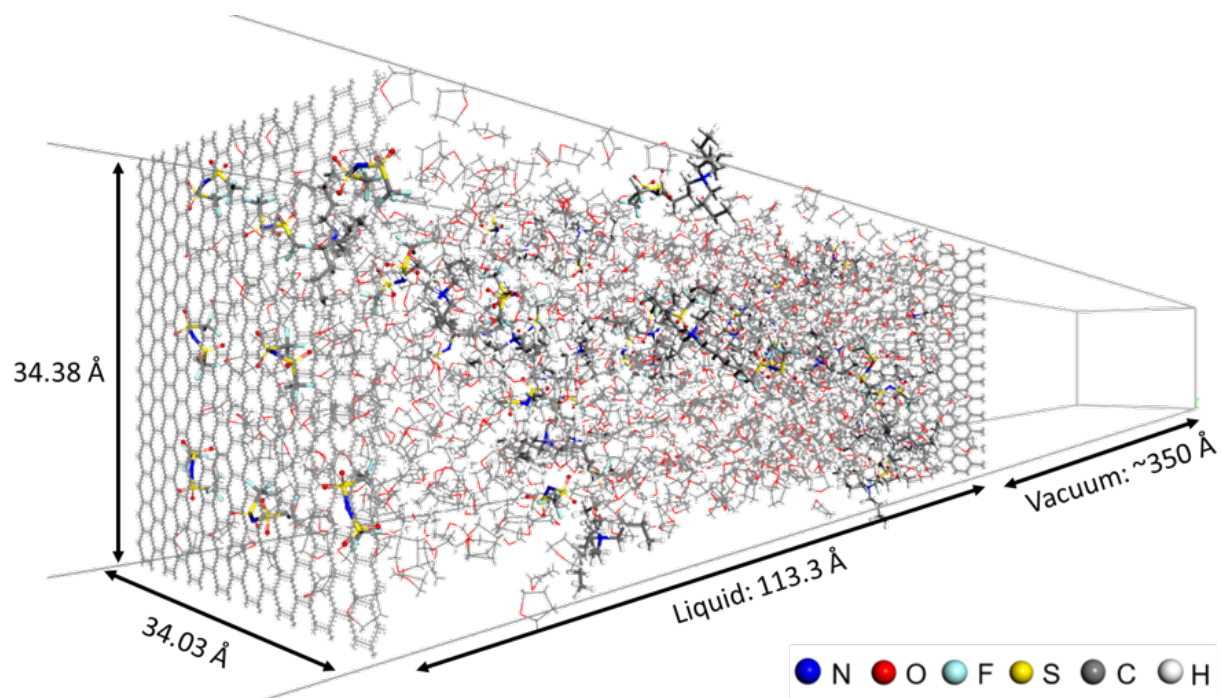
Schematic view of the MD simulation box

Figure S5: Snapshot at 4000 ps of TBATFSI electrolyte as an example of the geometry of the MD simulation box.
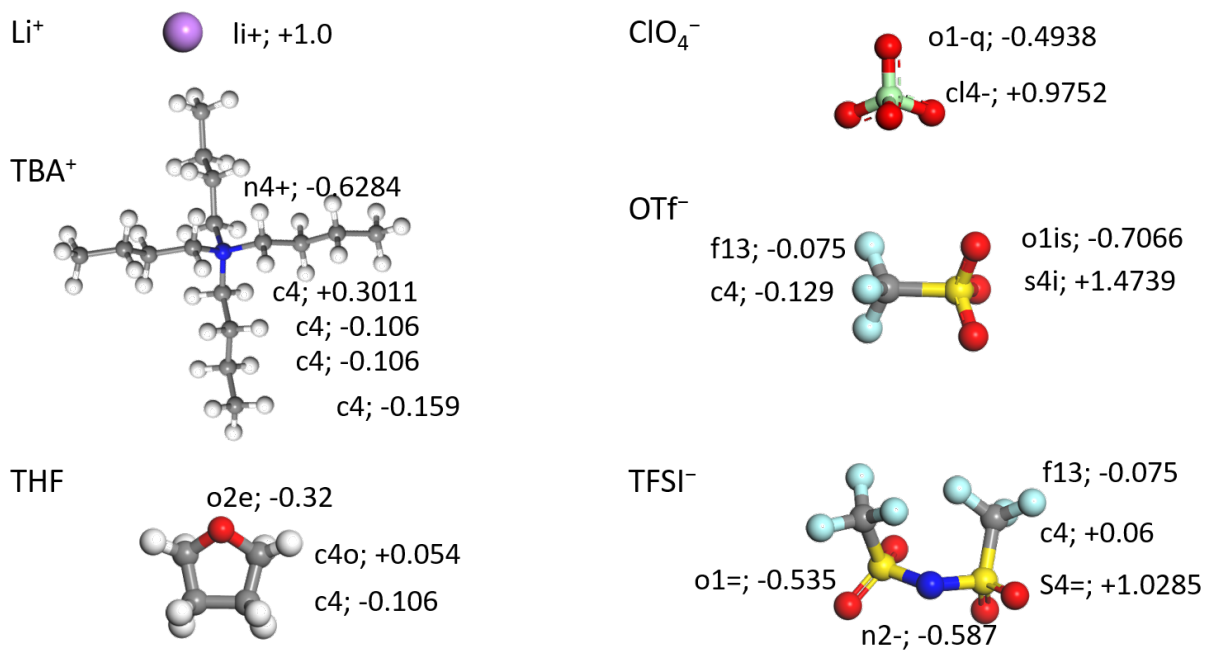
Force field details

Li⁺   li+; +1.0

TBA⁺

n4+; -0.6284

c4; +0.3011
c4; -0.106
c4; -0.106
c4; -0.159

THF

o2e; -0.32
c4o; +0.054
c4; -0.106

ClO_4^-

o1-q; -0.4938
cl4-; +0.9752

OTf⁻

f13; -0.075
c4; -0.129

o1is; -0.7066
s4i; +1.4739

TFSI⁻

f13; -0.075
c4; +0.06
o1=; -0.535
S4=; +1.0285
n2-; -0.587

Figure S6: Electrolyte species investigated in this work, including THF, Li⁺, TBA⁺, ClO_4^-, OTf⁻, and TFSI⁻. Representative atom forcefield types and atomic charges are given accordingly. The charges were assigned by the according COMPASSIII forcefield type. The forcefield type of hydrogen atoms were automatically assigned by the Forcite module in Materials Studio 2020, unless otherwise specified.

Simulated densities

Table S1: The densities of the bulk phases were computed from the last 600 ps of each 1 ns NPT trajectory using cubic boxes. Each system consists of 30 salt species and 800 THF molecules. The distance between the graphene slabs in the slab-geometry cells was adjusted to match the simulated densities of bulk solutions.

System	Bulk density (g/mL)	Salt molarity (mol/L)	Distance between slabs (Å)
$LiClO_4$	0.952	0.492	97.4
$TBAClO_4$	0.920	0.433	109.8
LiOTf	0.929	0.428	98.7
TBAOTf	0.944	0.485	111.1
LiTFSI	0.985	0.475	100.5
TBATFSI	0.962	0.419	113.3

DFT binding energy

The binding energies of cation-anion and cation-solvent interactions and anions were calculated by the Gaussian (G09) package using density functional theory (DFT).[1] The M06-2X/6-31+G(d,p) level of theory[2] along with the D3 dispersion correction[3] is used without applying the basis set superposition error (BSSE) correction. Their performance on describing noncovalent interactions[4] and binding energies of supramolecular complexes,[5] anions,[6,7] hydrogen-bonded ions,[8] and sulfuric acid containing clusters,[9] have been well discussed in the literature. As a common choice for calculating binding energies for similar systems, they have been used to calculate binding energies of different ions in organic solvents for battery electrolytes. 3 The energies were obtained from gas phase geometry optimization and the bonding energies are calculated as

$$\Delta E_{bonding} = E_{A-B} - (E_A + E_B)$$

To validate the force fields, the binding energies were calculated using the force fields also by the above equation, and compared with the DFT results.
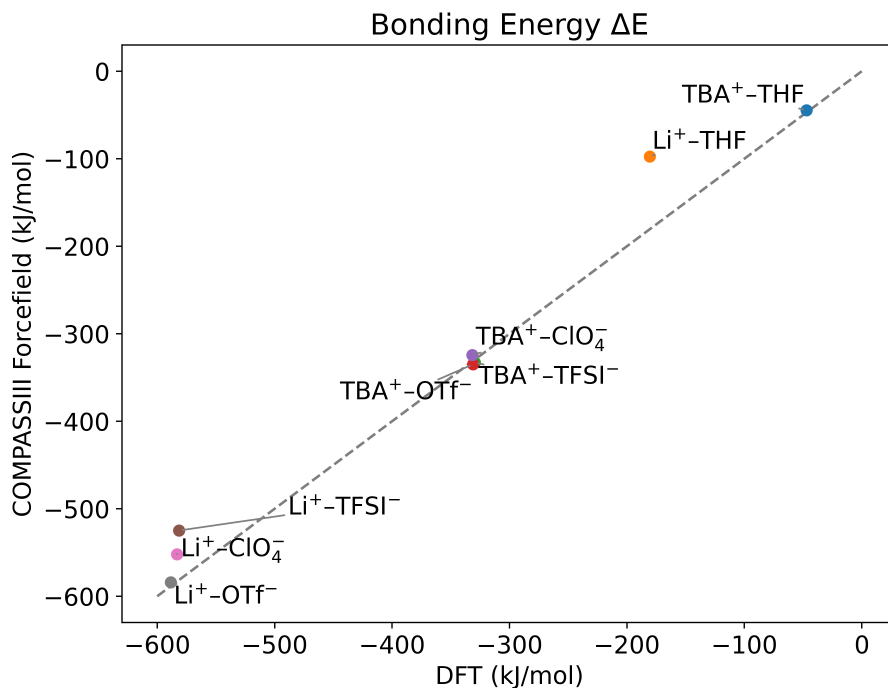

Figure S7: Bonding energies of ion pairs. Li^+ in general form stronger ionic bond compared to TBA^+. The DFT results and the forcefield results are consistent in terms of this trend.

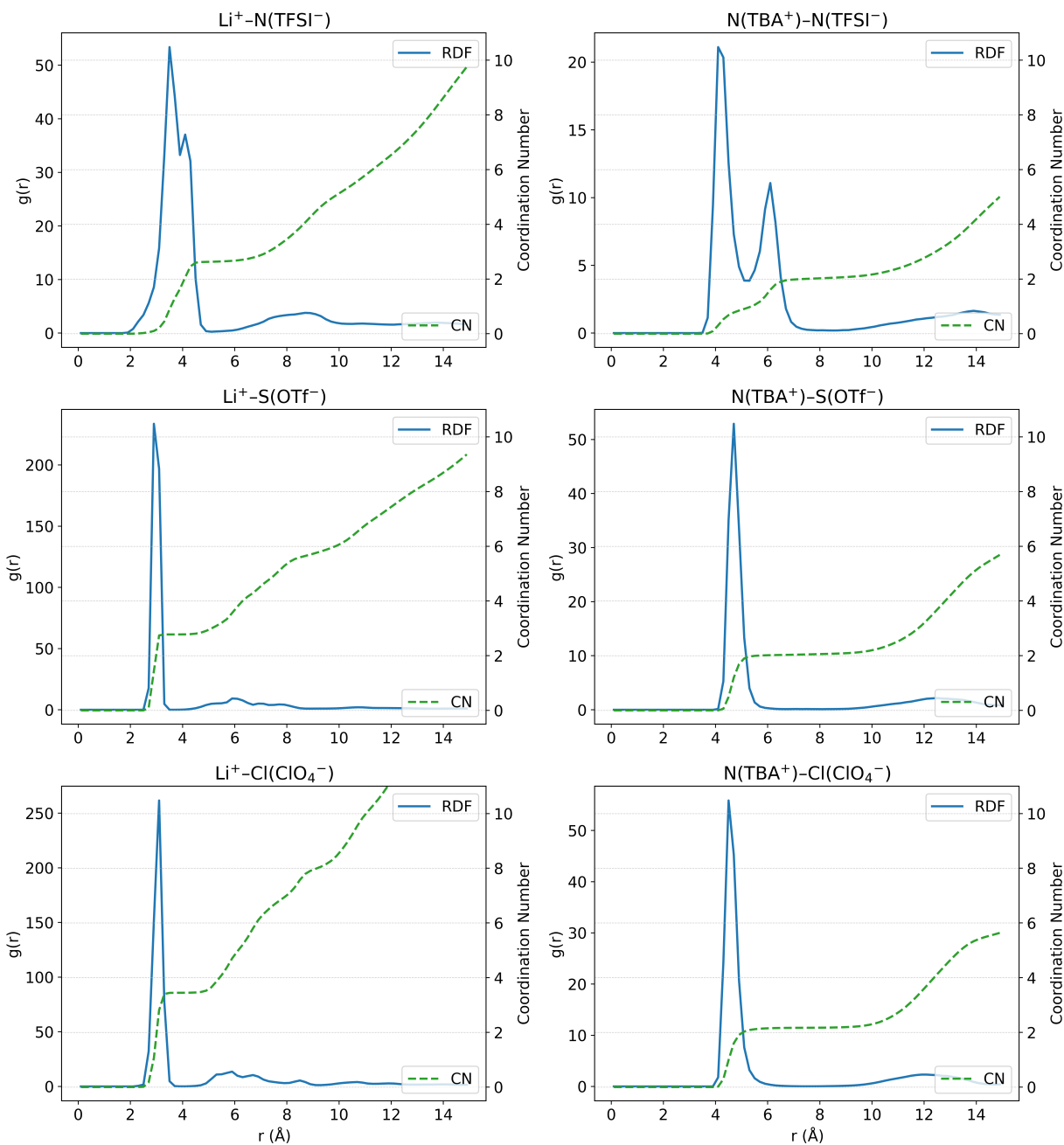**Radial distribution functions (RDF) in bulk phase**

Figure S8: Radial distribution function (RDF) $g(r)$ and coordination number (CN) plots of cation-anion association. The RDFs were calculated from the production runs of bulk phases using 0.2 Å bin size. The distance cutoffs to determine "free or coordinated" ions were based on the distance where the first RDF peak ends. The cutoff values are N(TBA$^+$)–N(TFSI$^-$): 7 Å, N(TBA$^+$)–S(OTf$^-$): 6 Å, N(TBA$^+$)–Cl(ClO$_4^-$): 6 Å, Li$^+$–N(TFSI$^-$): 5Å, Li$^+$–S(OTf$^-$): 3.5 Å, Li–Cl(ClO$_4^-$): 3.5 Å.
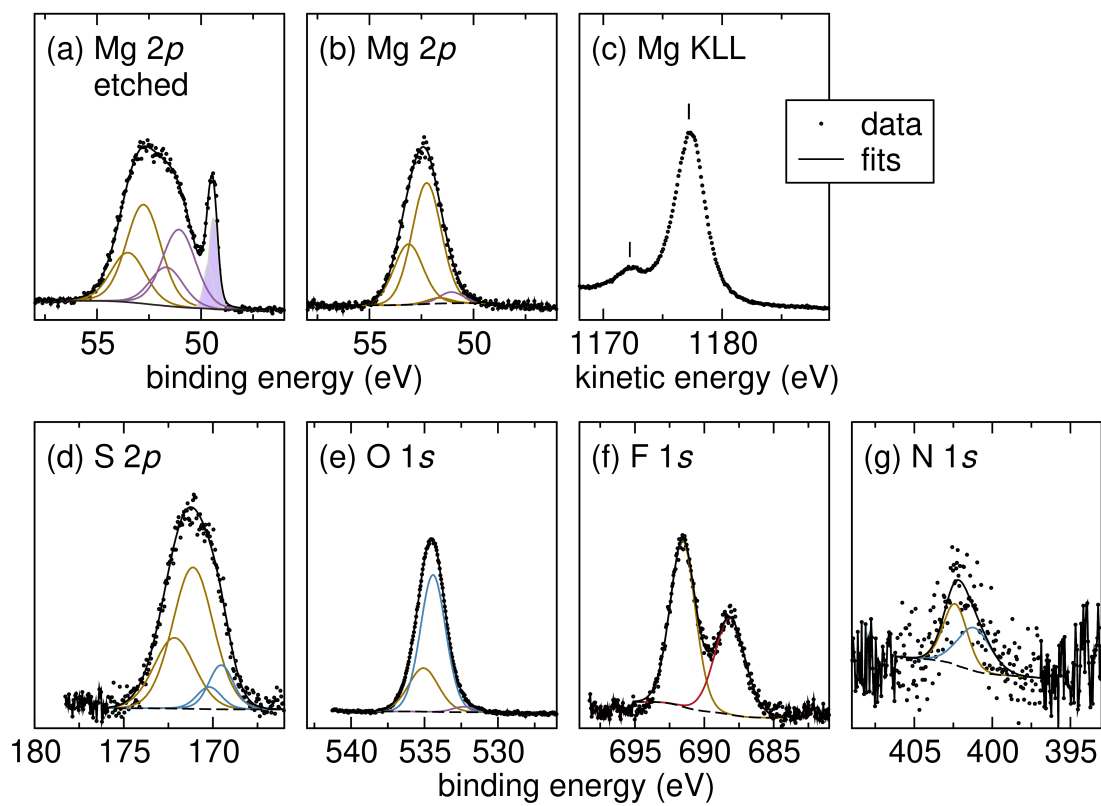
XPS data

Figure S9: X-ray photoelectron spectra of Mg electrodes after the LSV experiments in THF with TBATFSI as the supporting electrolyte.

Table S2: Peak assignments of the X-ray photoelectron spectra of Mg electrodes after the LSV experiments in THF with TBATFSI as the supporting electrolyte.

| Figure	Peak binding energy (eV)	Assignment
Figure S9a. Mg 2p	49.4	Mg^0
	51.1	MgO
	52.8	Mg(TFSI)$_2$/Mg(NSOCF$_3$)$_2$
Figure S9b. Mg 2p	51.1	MgO
	52.3	Mg(TFSI)$_2$/Mg(NSOCF$_3$)$_2$
Figure S9d. S 2p	169.5	Mg(NSOCF$_3$)$_2$
	171.1	Mg(TFSI)$_2$
Figure S9e. O 1s	532.3	MgO
	534.4	Mg(NSOCF$_3$)$_2$
	535.1	Mg(TFSI)$_2$
Figure S9f. F 1s	688.2	–CF$_2$
	691.5	–CF$_3$
Figure S9g. N 1s	401.2	Mg(NSOCF$_3$)$_2$
	402.4	Mg(TFSI)$_2$
	Peak kinetic energy (eV)	
Figure S9c. Mg KLL	1172.6	bulk plasmon
	1177.4	Mg^{2+}
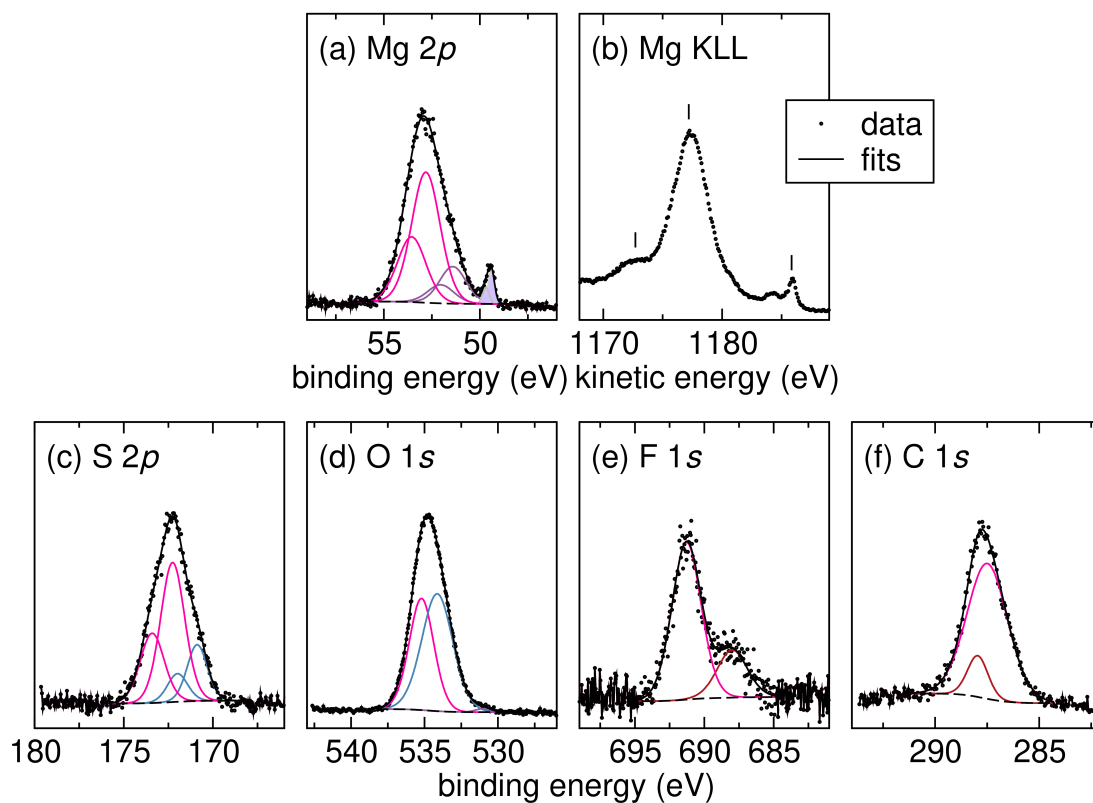
Figure S10: X-ray photoelectron spectra of Mg electrodes after the LSV experiments in THF with TBAOTf as the supporting electrolyte.

Table S3: Peak assignments of the X-ray photoelectron spectra of Mg electrodes after the LSV experiments in THF with TBAOTf as the supporting electrolyte.

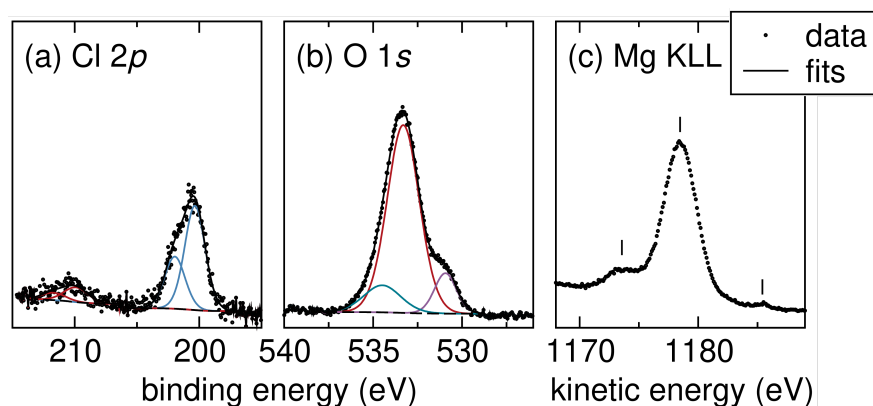| Figure	Peak binding energy (eV)	Assignment
Figure S10a. Mg $2p$	49.4	Mg^0
	51.4	MgO
	51.7	$Mg(OTf)_2/Mg(SO_2CF_3)_2$
Figure S10c. S $2p$	170.9	$Mg(SO_2CF_3)_2$
	172.3	$Mg(OTf)_2$
Figure S10d. O $1s$	531.0	MgO
	534.1	$Mg(SO_2CF_3)_2$
	535.2	$Mg(OTf)_2$
Figure S10e. F $1s$	688.0	$-CF_2$
	691.3	$-CF_3$
Figure S10f. C $1s$	287.5	$-CF_3$
	288.0	$-CF_2$
	Peak kinetic energy (eV)	
Figure S10b. Mg KLL	1172.9	bulk plasmon
	1177.4	Mg^{2+}
	1185.9	Mg^0

Figure S11: X-ray photoelectron spectra of Mg electrodes after the LSV experiments in THF with TBAClO$_4$ as the supporting electrolyte.

Table S4: Peak assignments of the X-ray photoelectron spectra of Mg electrodes after the LSV experiments in THF with TBAClO$_4$ as the supporting electrolyte.

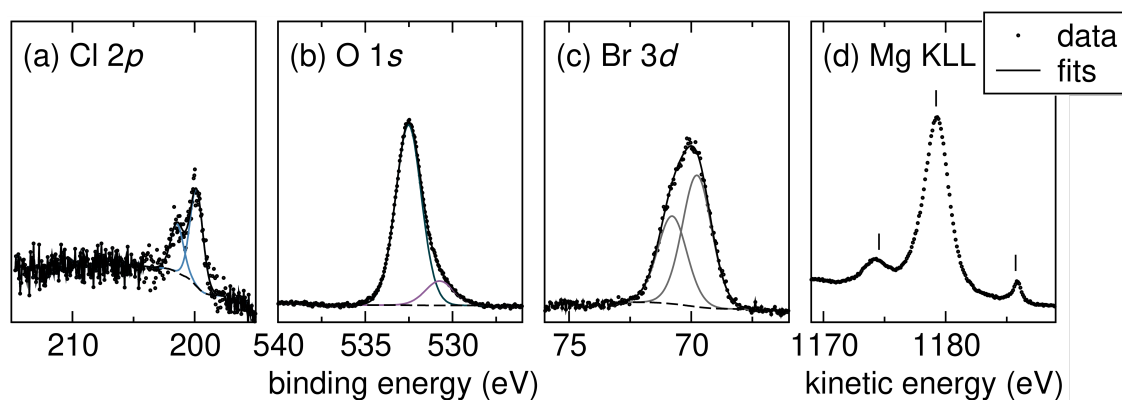| Figure	Peak binding energy (eV)	Assignment
Figure 5a. Mg 2p	49.4	Mg^0
	50.5	MgO
	51.4	MgCl$_2$/Mg(ClO$_4$)$_2$
Figure S11a. Cl 2p	200.4	MgCl$_2$
	209.9	Mg(ClO$_4$)$_2$
Figure S11b. O 1s	530.9	MgO
	533.3	Mg(ClO$_4$)$_2$
	534.5	C=O
Peak kinetic energy (eV)		
Figure S11c. Mg KLL	1173.9	bulk plasmon
	1178.9	Mg^{2+}
	1185.9	Mg^0

Figure S12: X-ray photoelectron spectra of Mg electrodes after the LSV experiments in THF with TBAClO$_4$/LiBr as the supporting electrolyte.

Table S5: Peak assignments of the X-ray photoelectron spectra of Mg electrodes after the LSV experiments in THF with TBAClO$_4$/LiBr as the supporting electrolyte.

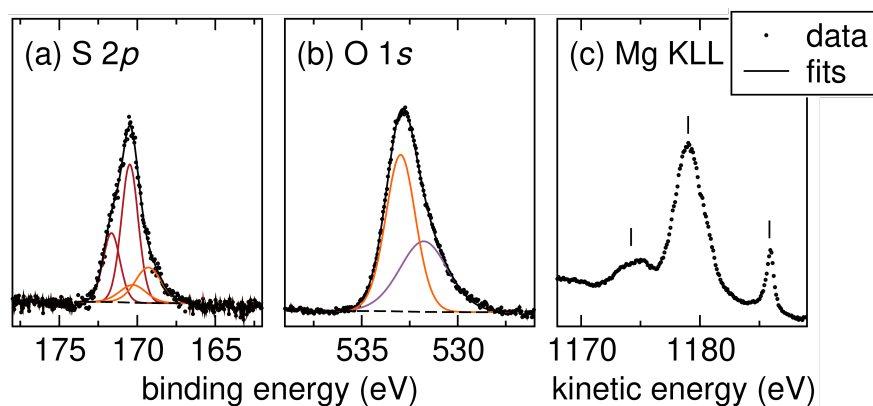| Figure	Peak binding energy (eV)	Assignment
Figure 5b. Mg 2p	49.4	Mg^0
	50.8	MgO
	51.2	MgBr$_2$
	51.8	MgCl$_2$
Figure S12a. Cl 2p	200.1	MgCl$_2$
Figure S12b. O 1s	530.7	MgO
	532.5	C–O
Figure S12c. Br 3d	69.9	MgBr$_2$
Peak kinetic energy (eV)		
Figure S12d. Mg KLL	1174.6	bulk plasmon
	1179.0	Mg^{2+}
	1185.8	Mg^0

Figure S13: X-ray photoelectron spectra of Mg electrodes after the LSV experiments in THF with TBAOTs as the supporting electrolyte.

Table S6: Peak assignments of the X-ray photoelectron spectra of Mg electrodes after the LSV experiments in THF with TBAOTs as the supporting electrolyte.

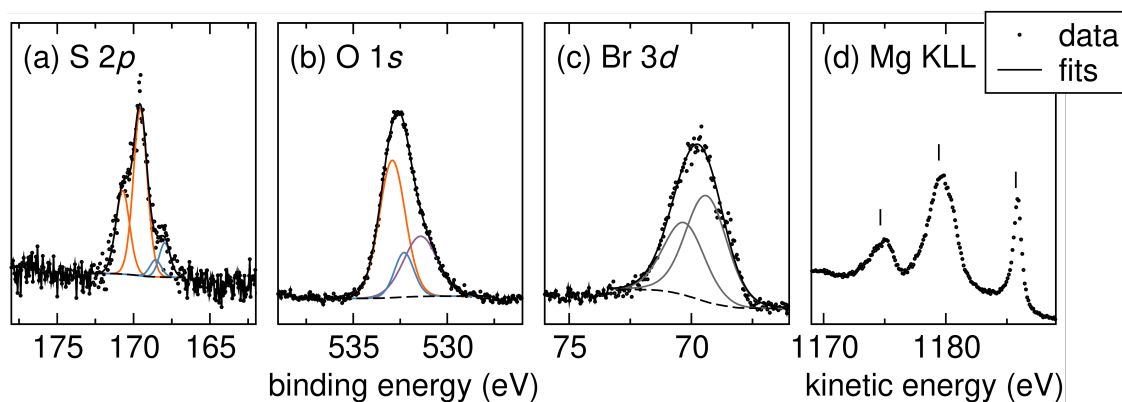| Figure	Peak binding energy (eV)	Assignment
Figure 5c. Mg $2p$	49.4	Mg^0
	50.9	MgO
	51.7	$Mg(OTs)_2$
Figure S13a. S $2p$	169.3	$Mg(OTs)_2$
	170.5	S–C
Figure S13b. O $1s$	531.8	MgO
	533.0	$Mg(OTs)_2$
Peak kinetic energy (eV)		
Figure S13c. Mg KLL	1174.4	bulk plasmon
	1179.2	Mg^{2+}
	1185.9	Mg^0

Figure S14: X-ray photoelectron spectra of Mg electrodes after the LSV experiments in THF with TBAOTs/LiBr as the supporting electrolyte.

Table S7: Peak assignments of the X-ray photoelectron spectra of Mg electrodes after the LSV experiments in THF with TBAOTs/LiBr as the supporting electrolyte.

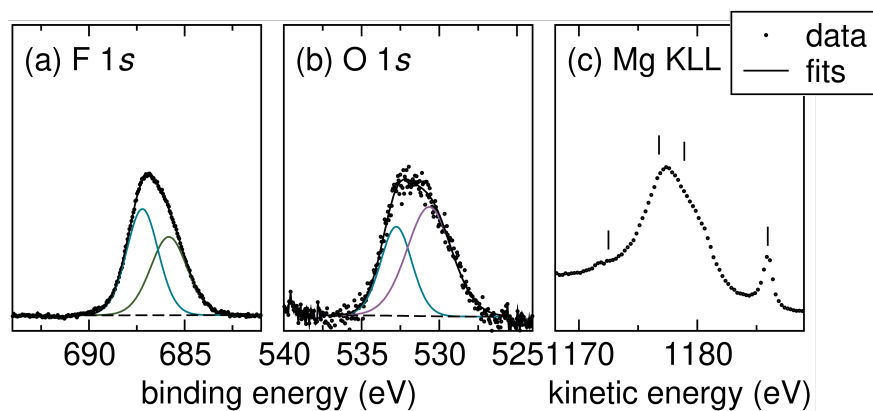| Figure	Peak binding energy (eV)	Assignment
Figure 5d. Mg $2p$	49.4	Mg^0
	50.3	MgO
	50.9	$MgBr_2$
	51.6	$Mg(OTs)_2/Mg(SO_2C_6H_4CH_3)_2$
Figure S14a. S $2p$	168.0	$Mg(SO_2C_6H_4CH_3)_2$
	169.6	$Mg(OTs)_2$
Figure S14b. O $1s$	531.4	MgO
	532.3	$Mg(SO_2C_6H_4CH_3)_2$
	532.9	$Mg(OTs)_2$
Figure S14c. Br $3d$	69.4	$MgBr_2$
	Peak kinetic energy (eV)	
Figure S14d. Mg KLL	1174.9	bulk plasmon
	1179.8	Mg^{2+}
	1185.9	Mg^0

Figure S15: X-ray photoelectron spectra of Mg electrodes after the LSV experiments in THF with TBAPF$_6$ as the supporting electrolyte.

Table S8: Peak assignments of the X-ray photoelectron spectra of Mg electrodes after the LSV experiments in THF with TBAPF$_6$ as the supporting electrolyte.

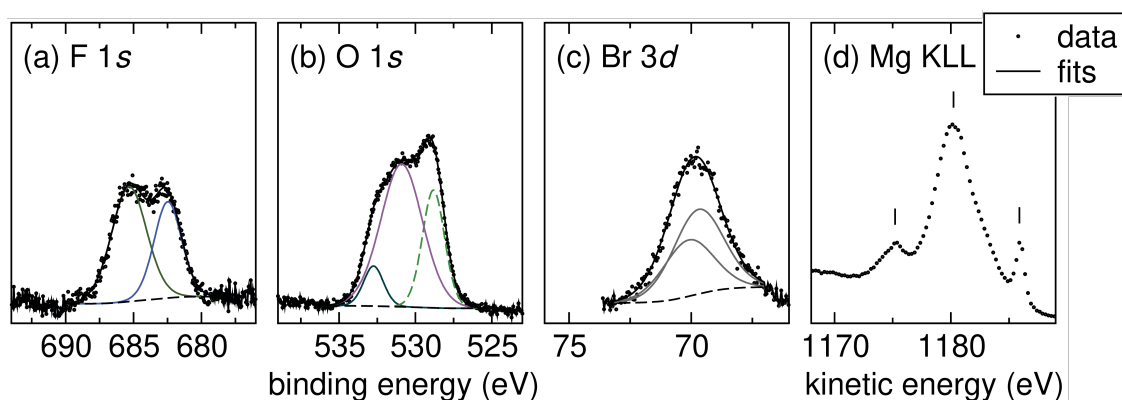| Figure	Peak binding energy (eV)	Assignment
Figure 5e. Mg 2p	49.4	Mg^0
	50.9	MgO
	52.5	MgF$_2$
Figure S15a. F 1s	685.7	MgF$_2$
	687.1	C–F
Figure S15b. O 1s	530.6	MgO
	532.7	C–O
	Peak kinetic energy (eV)	
Figure S15c. Mg KLL	1173.0	bulk plasmon
	1176.9	MgF$_2$
	1179.3	other Mg^{2+}
	1186.0	Mg^0

Figure S16: X-ray photoelectron spectra of Mg electrodes after the LSV experiments in THF with TBAPF$_6$/LiBr as the supporting electrolyte.

Table S9: Peak assignments of the X-ray photoelectron spectra of Mg electrodes after the LSV experiments in THF with TBAPF$_6$/LiBr as the supporting electrolyte.

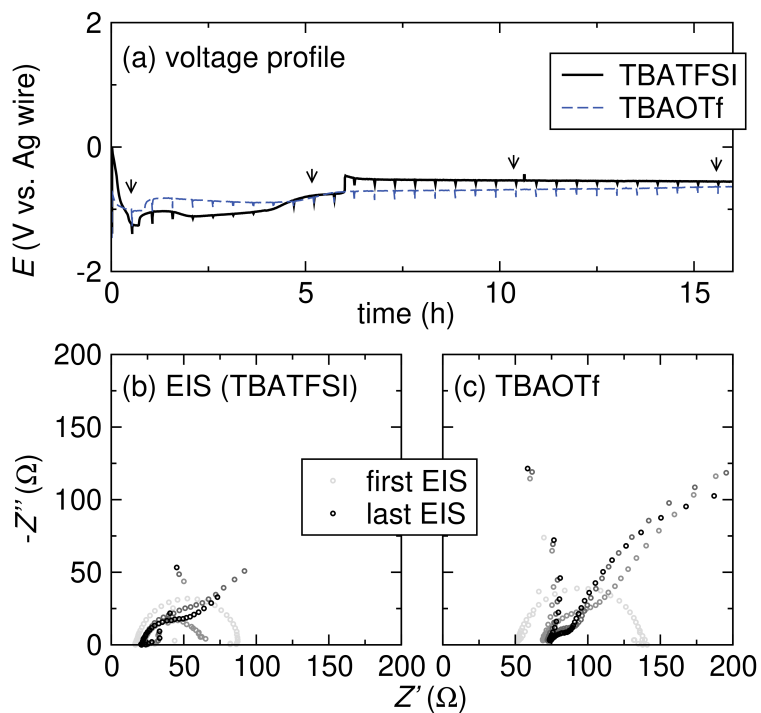| Figure	Peak binding energy (eV)	Assignment
Figure 5b. Mg 2p	49.4	Mg^0
	50.7	MgO
	51.0	MgBr$_2$/MgF$_2$
	48.3	Mn–O
Figure S16a. F 2p	682.5	MF
	685.3	MgF$_2$
Figure S16b. O 1s	528.8	Mn–O
	530.9	MgO
	532.7	C–O
Figure S16c. Br 3d	69.7	MgBr$_2$
Peak kinetic energy (eV)		
Figure S16d. Mg KLL	1174.9	bulk plasmon
	1180.5	Mg^{2+}
	1185.9	Mg^0

Figure S17: (a) Voltage profiles on the Mg working electrodes of the galvanostatic Mg stripping (j = 1 mA/cm^2) experiments in THF in the presence of 0.5 M tBuBr with 0.5 M TBATFSI or 0.5 M TBAOTf. EIS was performed every 30 min during the galvanostatic Mg stripping experiments. EIS of the Mg working electrodes in (b) 0.5 M TBATFSI electrolyte, and (c) 0.5 M TBAOTf electrolyte. Only the 1st, 10th, 20th, 30th EIS are shown here. The time points are indicated by arrows in (a)
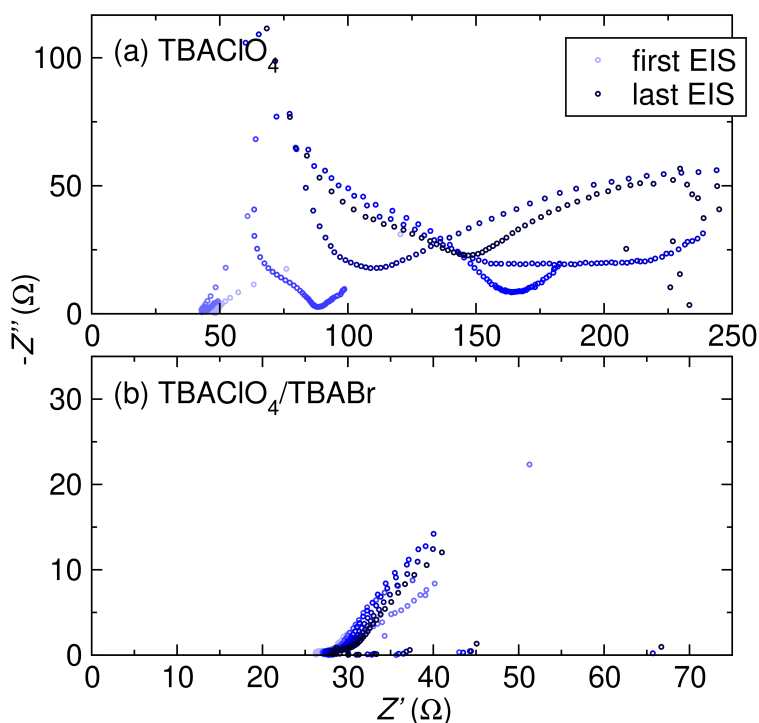
Figure S18: EIS of the Mg working electrodes during galvanostatic Mg stripping in the presence of 0.5 M tBuBr in (a) 0.5 M TBAClO$_4$ electrolyte, and (b) 0.25 M TBAClO$_4$ + 0.25 M TBABr electrolyte. Comparing (a) and (b), the Mg interface is more stable in TBAClO$_4$/LiBr electrolyte.

References

(1) Frisch, M. J. et al. Gaussian09 Revision E.01. Gaussian Inc. Wallingford CT 2009.

(2) Zhao, Y.; Truhlar, D. G. The M06 Suite of Density Functionals for Main Group Thermochemistry, Thermochemical Kinetics, Noncovalent Interactions, Excited States, and Transition Elements: Two New Functionals and Systematic Testing of Four M06-class Functionals and 12 Other Functionals. *Theor. Chem. Account.* **2008**, *120*, 215–241.

(3) Grimme, S.; Ehrlich, S.; Goerigk, L. Effect of the Damping Function in Dispersion Corrected Density Functional Theory. *J. Comput. Chem.* **2011**, *32*, 1456–1465.

(4) Goerigk, L.; Hansen, A.; Bauer, C.; Ehrlich, S.; Najibi, A.; Grimme, S. A Look at the Density Functional Theory Zoo with the Advanced GMTKN55 Database for General Main Group

Thermochemistry, Kinetics and Noncovalent Interactions. *Phys. Chem. Chem. Phys.* **2017**, *19*, 32184–32215.

(5) Antony, J.; Sure, R.; Grimme, S. Using Dispersion-Corrected Density Functional Theory to Understand Supramolecular Binding Thermodynamics. *Chem. Commun.* **2015**, *51*, 1764–1774.

(6) Walker, M.; Harvey, A. J. A.; Sen, A.; Dessent, C. E. H. Performance of M06, M06-2X, and M06-HF Density Functionals for Conformationally Flexible Anionic Clusters: M06 Functionals Perform Better than B3LYP for a Model System with Dispersion and Ionic Hydrogen-Bonding Interactions. *J. Phys. Chem. A* **2013**, *117*, 12590–12600.

(7) Sandler, I.; Sharma, S.; Chan, B.; Ho, J. Accurate Quantum Chemical Prediction of Gas-Phase Anion Binding Affinities and Their Structure-Binding Relationships. *J. Phys. Chem. A* **2021**, *125*, 9838–9851.

(8) Rodrigues-Oliveira, A. F.; M. Ribeiro, F. W.; Cervi, G.; C. Correra, T. Evaluation of Common Theoretical Methods for Predicting Infrared Multiphotonic Dissociation Vibrational Spectra of Intramolecular Hydrogen-Bonded Ions. *ACS Omega* **2018**, *3*, 9075–9085.

(9) Myllys, N.; Elm, J.; Kurtén, T. Density Functional Theory Basis Set Convergence of Sulfuric Acid-Containing Molecular Clusters. *Comput. Theor. Chem.* **2016**, *1098*, 1–12.